

Black shales contamination and depositional paleoenvironment during the Early Aptian OAE 1a in the Eastern Russian Platform

SVETLANA O. ZORINA



The most pernicious consequences of the Early Aptian Oceanic Anoxic Event (OAE) 1a in the North-Eastern Peri-Tethys for benthic microfauna were oxygen decrease and the onset of sulphidic conditions, related to toxic enrichment in heavy metals which can be regarded as one of the main causes for biota distress and even their disappearance. Twenty-nine samples from the Tatar-Shatrasahy borehole located in the Ulyanovsk-Saratov Trough (Eastern Russian Platform) were studied to estimate the extent of anoxia using trace element redox proxies and pyrite framboid morphology and distribution. The degree of contamination in toxic metals (As, Cd, Se, Pb, Zn, Ni, Mo, Cu, V, and W) is estimated for the Lower Aptian OAE 1a-related black shales of the Ulyanovsk Formation and compared with the results obtained for the Late Jurassic OAE-related black shales of the Promzino Formation and host mudrocks. The relationships between benthic foraminiferal abundance and diversity and black shales contamination in toxic metals are evaluated. Extreme contamination of the OAE 1a-related black shales in Mo and Cd in conjunction with the absence of oxygen could result in conditions not suitable for benthic foraminifers dwelling. The key species *Mjatlukaena aptiensis* (Mjatl.) is regarded to be one of the toxic-resistant species that successfully recovered from the OAE 1a anoxic stress. Comparing to the Late Jurassic OAE, the integrated data indicate moderately contaminated black shales and mainly dysoxic conditions under which habitat conditions were not completely detrimental for benthic foraminifers. The most toxic-resistant species was *Lenticulina infravolgaensis* (Furs. et Pol.). • Key words: OAE 1a; Aptian; anoxia; black shales; Peri-Tethys; foraminiferal abundance.

ZORINA, S.O. 2022. Black shales contamination and depositional paleoenvironment during the Early Aptian OAE 1a in the Eastern Russian Platform. *Bulletin of Geosciences* 97(1), 123–140 (6 figures, 6 tables, electronic supplement). Czech Geological Survey, Prague. ISSN 1214-1119. Manuscript received May 24, 2020; accepted in revised form November 8, 2021; published online November 22, 2021; issued January 23, 2022.

Svetlana O. Zorina, Institute of Geology and Petroleum Technologies, Kazan Federal University, 4/5 Kremlyovskaya Str., Kazan, Russian Federation 420008; svzorina@yandex.ru

Late Jurassic–Late Cretaceous is considered a time of increasing temperatures and “greenhouse conditions” (Scotese 2016). This period is marked by several episodes of widespread anoxia and enhanced productivity in the oceans (Jenkyns 2010, Scotese 2014), resulting in black shale deposits known in the Cretaceous as Oceanic Anoxic Events (OAE) (Schlanger & Jenkyns 1976). The Early Aptian OAE 1a (Selli Event, ~120 Ma) lasting ~1–1.4 Ma (Li *et al.* 2008, Malinverno *et al.* 2010) coincided with both the beginning of significant warming and a short-term drop in $\delta^{13}\text{C}$ values in marine carbonates (*e.g.*, Menegatti *et al.* 1998, Zakharov *et al.* 2013). The event could be caused by an activation of large igneous provinces (Larson & Erba 1999, Tejada *et al.* 2009, Keller *et al.* 2011, Percival *et al.* 2021) or release of methane gas hydrate trapped in oceanic sediments (*e.g.*, Jahren *et al.* 2001, Van Breugel *et al.* 2007) leading to sudden addition of isotopically light volcanic CO_2 to the atmosphere and oceans. Similar events are known from the Jurassic, *e.g.*

the Toarcian anoxic event (French *et al.* 2014) and the “Late Jurassic anoxic event” (Trabucho-Alexandre *et al.* 2012, Nozaki *et al.* 2013).

At the moment, deposits rich in organic matter (OM) are of increasing interest since they are a potential source of hydrocarbons and an indicator for climate and environmental changes, but also may comprise itself a source of greenhouse gases, such as methane (Maksyutova *et al.* 2018).

There is a general acceptance confirmed by the results from the Tethys, Atlantic, and Pacific oceans, North Sea, Russian Platform, Lower Saxony, and many other basins that major warming characterized OAE 1a (Selli Event), which began before and reached a maximum during initial OAE 1a (*e.g.*, Erba *et al.* 2010, Zakharov *et al.* 2013, Bottini *et al.* 2015). The rest of the OAE 1a interval was marked by subsequent “cold snap”, and a further cooling took place when the uppermost part of the organic carbon-rich level was deposited (*e.g.*, Bottini *et al.* 2015).

Considering the anoxic events have been well studied and described in many studies, the general presentation of the consequences of these events is characterized by temperature maximum, hydrothermal and volcanic driven ocean fertility increase, extensive transgressions, stagnation of hydrodynamic regime of basins, and stratification of water masses, decrease in dissolved oxygen in the water, biotic crisis, and conditions under which the OM does not oxidize and is preferably preserved in the sediments (Schlanger & Jenkyns 1976, Jenkyns 2010).

The main feature of benthic foraminiferal assemblages during the OAE 1a in different regions of the Tethys Ocean is a dramatic decrease in both diversity and abundance or their total absence (Premoli Silva *et al.* 1999, Friedrich 2010, Moosavizadeh *et al.* 2014, von Barga & Lehmann 2014). Together with the above-mentioned oxygen decrease and wide-spread hydrogen sulphide contamination, the most pernicious outcome for benthic microfauna could be a contamination of sediments by toxic metals (TM) (Murray 2006, Galiakberov *et al.* 2018).

The degree and extent of toxic-metal pollution in recent sediments as a result of human activities has been one of the main topics studied in environmental geochemistry. In addition to anthropogenic metal inputs, high levels of potentially toxic elements are present in natural geochemical materials, such as Cd, Mo, and other heavy metals in black shales throughout the world (*e.g.*, Atkinson 1967, Vine & Tourtelot 1970, Lund *et al.* 1981, Lee *et al.* 1998, Poňavič *et al.* 2006, Ketris & Yudovich 2009).

One of the problems to solve was to estimate the extent of anoxia and the degree of the TM contamination

in the Lower Aptian OAE 1a-related black shales from the epeiric sea of the North-Eastern Peri-Tethys (Eastern Russian Platform) and to compare the results with those in the Late Jurassic OAE-related black shales and host mudrocks. The second one concerns the relationships between benthic foraminiferal abundance and diversity and black shales contamination in TM.

Bulk-rock samples of bituminous rocks from two anoxic levels (the Early Aptian Ulyanovsk Formation [Fm] and the Middle Volgian Promzino Fm) from the Tatar-Shatrashany borehole (Eastern Russian Platform) were studied, to address the problem under discussion.

Finally, to generalize the data obtained the task was to provide a paleoenvironmental model for the pre-OAE 1a, OAE 1a, and post-OAE 1a conditions in the North-Eastern Peri-Tethys, including paleoclimate and sea-level fluctuations.

Geologic setting and paleogeography

Twenty-nine cores of bituminous rocks from two anoxic levels and host mudrocks, 210 m in total thickness were studied from the Tatar-Shatrashany borehole which was drilled for geological survey purposes in the Republic of Tatarstan, Russian Federation. It is located in the eastern part of European Russia, 70 km northwest of the city of Ulyanovsk (E 47.383122°, N 54.554399°) (Fig. 1).

Rocks of the Tatar-Shatrashany borehole were deposited on the North-Eastern Peri-Tethys (Eastern Russian Platform) within an epeiric sea acting as a marine strait connecting the Tethys Ocean with the Boreal-Arctic

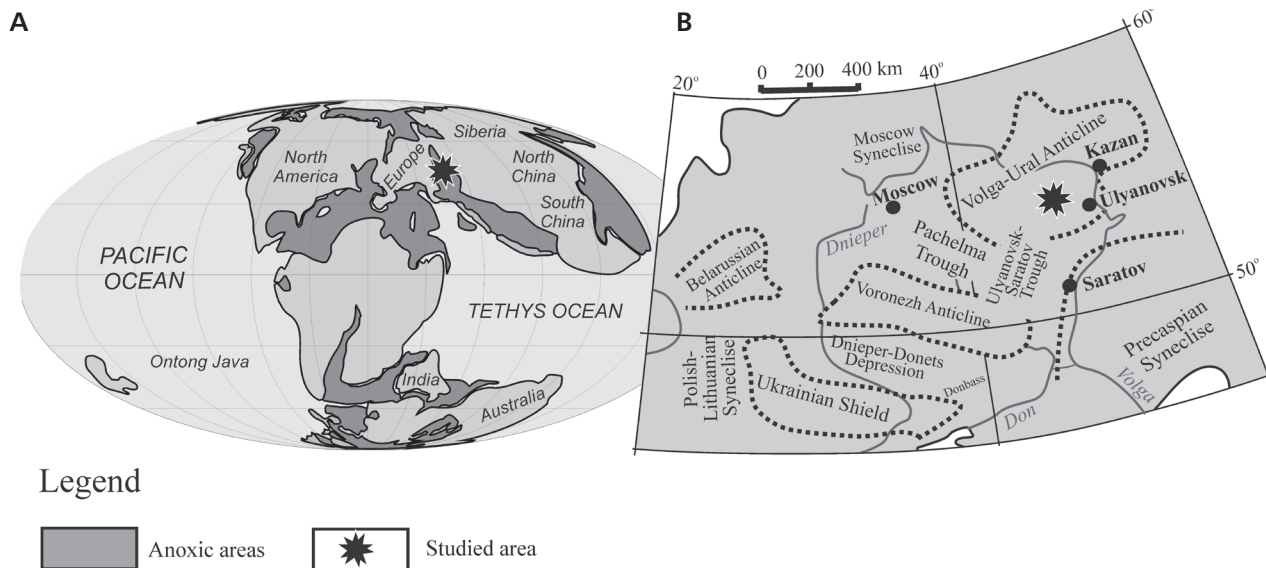
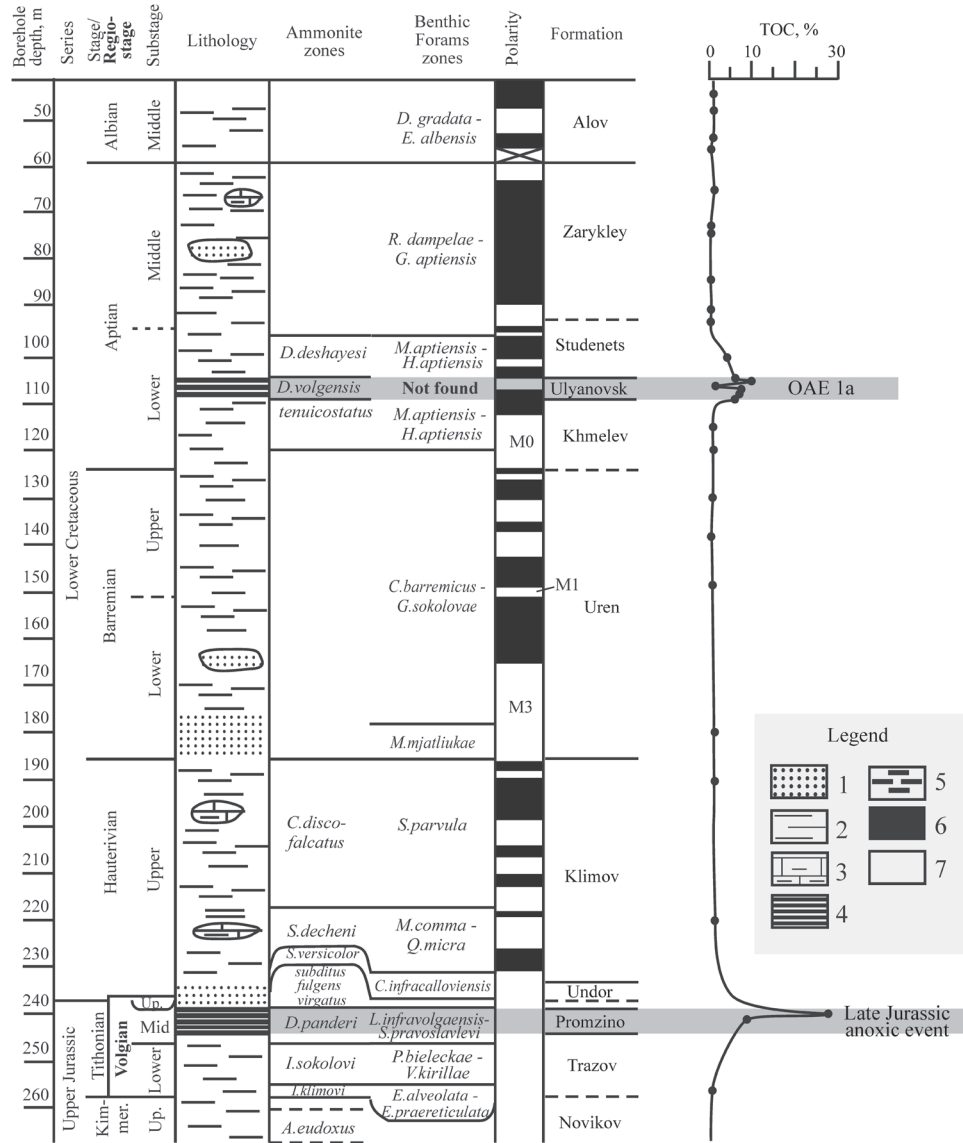


Figure 1. Location of studied area: A – on the Early Aptian paleogeographic map (simplified from Scotese 2014); B – on the tectonic scheme of the Eastern Russian Platform (simplified from Olfieriev *et al.* 2008).

Figure 2. Upper Jurassic–Lower Cretaceous strata of the Tatar-Shatrashany Borehole (Eastern Russian Platform) (Zorina 2016) and TOC content of rocks (Zorina *et al.* 2020). Legend: 1 – sandstones; 2 – mudrocks; 3 – marlstones; 4 – black shales; 5 – bituminous mudrocks; 6 – normal polarity; 7 – reverse polarity.



Sea during the Early Aptian (Fig. 1A) (Scotese 2014). Palaeolatitude of the site determined using <http://paleolatitude.org> for the age of 120 Ma is 45.34°N. Seawater palaeotemperatures calculated from oxygen isotopic analyses of aragonite bivalve shells and heteromorphic ammonites from the Lower Aptian black shales of the Eastern Russian Platform showed extremely high values 24–33.2 °C (Zakharov *et al.* 2013).

Tectonically, the section belongs to the Ulyanovsk-Saratov Trough (Fig. 1B) which stretches in the eastern part of the Russian Platform for more than 850 km being filled with Middle Jurassic–Paleogene deposits (Olferiev *et al.* 2008).

The Upper Jurassic–Lower Cretaceous strata of the Tatar-Shatrashany borehole consist of the Upper Kimmeridgian–Middle Volgian (Upper Tithonian) and the Upper Hauterivian–Middle Albian successions (Zorina

2014, 2016). The Upper Jurassic sequence comprises bluish-gray and light gray carbonate mudrocks and marlstones, up to 25 m in thickness (Upper Kimmeridgian Novikov Fm and Lower–Middle Volgian Trazov Fm) which are overlapped by black shales of the Middle Volgian Promzino Formation. The Promzino Fm consists of dark brown thinly laminated bituminous shales and bituminous mudrocks, 6 m in thickness. Benthic foraminifers from the Upper Jurassic *Lenticulina infravolgaensis* – *Saracenaria pravoslavlevi* Zone are found in the Promzino black shales (Fig. 2). It is overlaid by greenish-gray sandstones, with phosphorite pebbles, 0–1.5 m in thickness (Upper Volgian Undor Fm) (Zorina 2007) (Fig. 2).

The total organic carbon (TOC) content in the Promzino black shales varies from 8.4 to 27.3% (Zorina 2009, 2014) (Fig. 2). This organic carbon-rich formation is regarded as a manifestation of the Late Jurassic OAE,

the sedimentary expressions of which are reported from different regions of the world; in particular, the Bazhenov Fm of the West Siberian Platform (Ulmishek 2003) and voluminous sulphide deposition in Panthalassa (Nozaki *et al.* 2013).

The Lower Cretaceous (Upper Hauterivian–Middle Aptian and Middle Albian) deposits are presented by highly bioturbated dark gray, mostly carbonate-free mudrocks, with rare interlayers of quartz sandstones. The thickness of the Upper Hauterivian Klimov Fm is more than 60 m, of the Barremian Uren Fm is more than 40 m, of the Aptian Khmelev, Ulyanovsk, Studenets, and Zarykley formations is about 90 m, and of the Albian Alov Fm is up to 130 m (Fig. 2, Tab. 1).

Importantly, the Lower Aptian black shales (Ulyanovsk Fm), 4.2 m in thickness (Fig. 2), are reported to correlate with OAE 1a (Gavrilov *et al.* 2002, Zorina *et al.* 2017). The Ulyanovsk Fm consists of dark brown thinly-laminated bituminous mudrocks (1–5 mm thick) with pyrite interlayers, composed of high-carbon closely-packed pyrite framboids indicating dysoxic conditions (Zorina *et al.* 2017). The TOC values vary between 6.1–10.0%. The black shales are interbedded by concretionary limestone, 1.2 m in thickness, with the TOC content of 1.3% (Fig. 2) (Zorina *et al.* 2020). Benthic foraminifers are abundant in the succession studied, except the Lower Aptian black shales where they were not found (Fig. 2).

Methods

Trace element analyses (V, Ni, Cu, Zn, As, Se, Mo, Cd, W, Pb, U, and Th) of twenty-nine bulk-rock samples from the Tatar-Shatrashany core were undertaken using an inductively coupled plasma mass spectrometer iCAP Qc (ThermoFisher Scientific, Germany). The obtained concentration values were recalculated to the initial concentration considering the empty sample, sample mass, and dilution of the solution. Additionally, concentrations of Al were investigated in the same samples that were used for ICP-MS using the S8 Tiger X-ray fluorescence wave-dispersion spectrometer (Bruker, Germany). The obtained spectrum was processed by the fundamental parameter's method, and automatic recognition errors.

Redox-sensitive element concentrations and their ratios (Mo, Mo/TOC, U/Th, U_{au} expressed as $U - \text{Th}/3$, V/Al, U/Al, Mo/Al, TOC/ P_{tot}) were used for estimating the degree of the anoxic condition.

Scanning electron microscope method was applied to determine pyrite framboids in six samples from both Ulyanovsk and Promzino black shales and when present, their size distribution was measured. The surface of the natural sample chip was examined with an XL-30 ESEM

scanning electron microscope. Microprobe analysis of the element composition at selected points of the sample was carried out with an energy-dispersive X-ray spectrometer.

The analyses were conducted at the Institute of Geology and Oil and Gas Technologies, Kazan Federal University (Russia).

The quantitative treatment of the diameters of pyrite framboids was used as an additional tool for the reconstruction of the redox conditions of the marine environment (Wignall *et al.* 2005, Bond & Wignall 2010).

To estimate the extent of sediment contamination in TM, ten trace elements identified as highly hazardous (As, Cd, Se, Pb, Zn), moderately hazardous (Ni, Mo, Cu), and low hazardous (V, W) metals according to Russian ecological Standard (Vodyanitskii 2012) were taken for further evaluation.

Geo-accumulation index (I_{geo}) is used as a quantitative measure of heavy metal pollution in aquatic sediments (Müller 1969) calculated by comparing current concentrations with geochemical background value metal in the Upper Continental Crust (Rudnick & Gao 2003), where, C_n – concentration of metal in sediment; B_n – background concentration of metal in the Upper Continental Crust (Rudnick & Gao 2003); 1.5 – a factor used to minimize the effect of possible variations in the background values which may be due to lithological variations in the sediments.

According to Müller (1969) seven different classes of I_{geo} values are established (Tab. 1).

Table 1. Different classes of I_{geo} values (Müller 1969).

Class	I_{geo} values	Sediment quality
0	≤ 0	Uncontaminated
1	0–1	Uncontaminated to moderately contaminated
2	1–2	Moderately contaminated
3	2–3	Moderately to heavily contaminated
4	3–4	Heavily contaminated
5	4–5	Heavily to extremely contaminated
6	≥ 5	Extremely contaminated

Measurement of foraminiferal abundance and diversity was provided using the results of microfaunal analysis (Zorina & Startseva 2010) of twenty-nine core samples from the same depth as those for geochemical analyses. The number of species of benthic foraminifers per 100 g of rock for each sample was taken from the microfaunal analysis performed by the paleontologist G.N. Startseva, and recalculated to the number of specimens per 1 m². Both data were used in constructing quantitative curves in order to study foraminiferal abundance and diversity throughout the section.

Results

Trace elements redox proxies

Raw geochemical data including the concentrations of TM and Al for the Upper Jurassic–Lower Cretaceous rocks from the Tatar-Shatrashany section are given in Table 2. The black shales of the Promzino and Ulyanovsk formations show considerable Mo and Mo/TOC enrichment (Tab. 3, Fig. 3), with Promzino shales having Mo values in the 22–24 ppm range, whereas the Ulyanovsk shales have higher values, some in excess of 140 ppm. The lowest Mo concentrations (5.7 ppm or less) occur in the organic carbon-poor Novikov and Trazov marls and Klimov–Alov mudrocks. The Mo/TOC ratios of the Ulyanovsk shales are of the highest values varying from 10.3 to 41.6, whereas the Promzino shales display much lower values in the 0.8–2.9 range. The host organic carbon-poor rocks have a wide range of values, thus mudrocks from the Lower Cretaceous formations show Mo/TOC values in the 0.4–3.1 range, the Upper Jurassic marls display the 3–9.1 range.

Both Promzino and Ulyanovsk black shales have U/Th ratios from 1.4 to 2.6, while the host marls and

mudrocks show values in the 0.1–0.5 range (Table 3; Fig. 3).

The U_{au} content in the Promzino black shales is found in the 11.1–11.9 ppm range, while the Ulyanovsk black shales show 5.7–17.8 ppm. It is noteworthy that the organic carbon-poor rocks reveal consistently low values of the U_{au} about 2.4–2.8 ppm (Tab. 3, Fig. 3).

Both organic carbon-rich formations display V/Al, U/Al, and Mo/Al ratios in the 34.7–48.3, 1.8–4.5, and 26.5–126.5 ranges, respectively, whereas organic carbon-poor strata show these ratios in the 15.4–28.8, 0.2–1.0, and 2.2–72.2 ranges, respectively (Tab. 3, Fig. 3).

The Promzino and Ulyanovsk black shales show TOC/P ratio in the 74.6–112 and 26.5–125 ranges, respectively whereas the host mudrocks display much lower values in the 2.2–72.2 range (Tab. 3, Fig. 3).

Pyrite framboids shape and distribution

Pyrite framboids are found in both Promzino and Ulyanovsk black shales (Fig. 4). Most framboids have close-packed shape, but the Promzino black shales contain both close-packed and disintegrating framboids (Fig. 4).

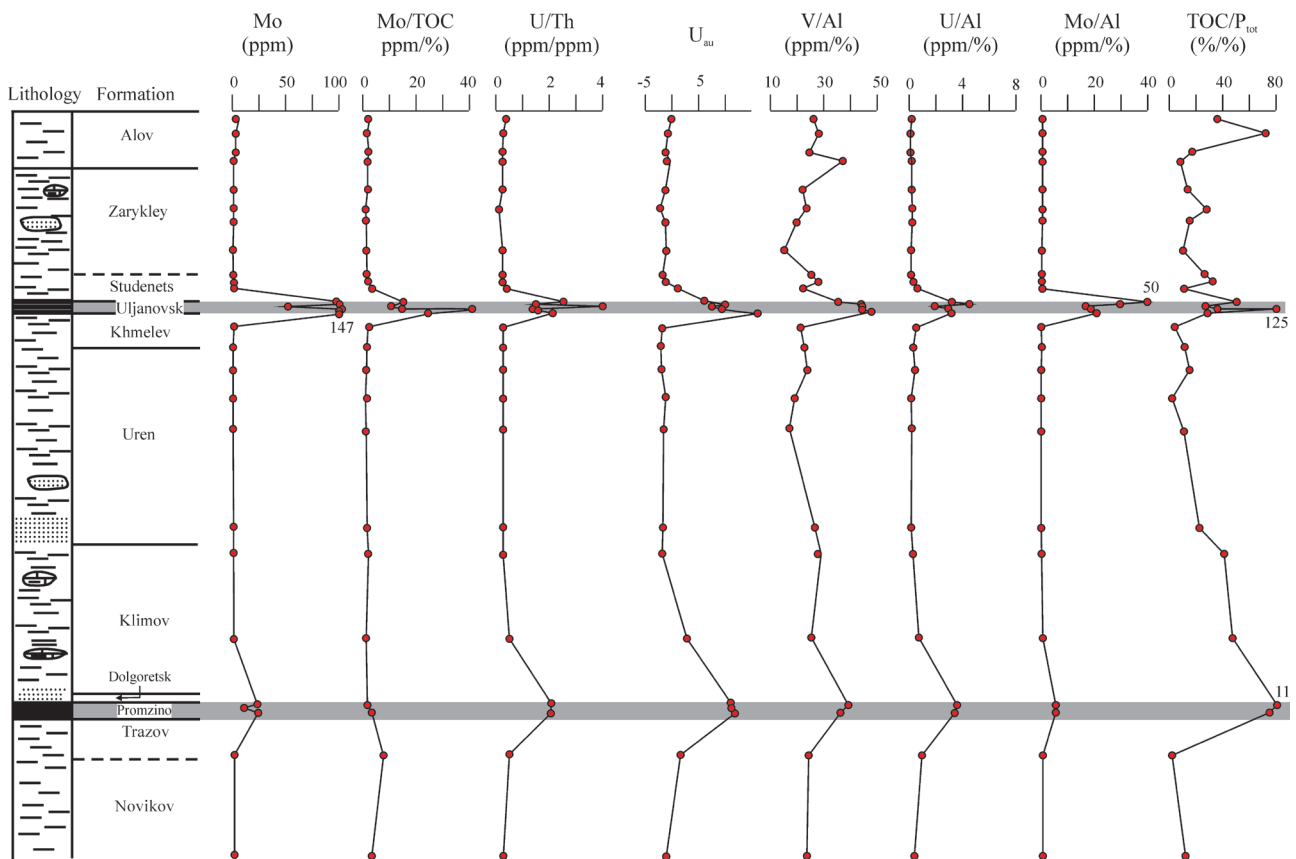


Figure 3. Stratigraphic variations of redox proxies for the Tatar-Shatrashany section. Gray stripes trace the organic carbon-rich intervals.

Table 2. Raw geochemical data for the Upper Jurassic–Lower Cretaceous rocks from the Tatar-Shatrashany section.

Sample	Depth (m)	Formation	Lithology	V (ppm)	Ni (ppm)	As (ppm)	Se (ppm)	Mo (ppm)	Cd (ppm)	W (ppm)	U (ppm)	Th (ppm)	Al ₂ O ₃ (%)
1/3	43		Dark gray mudrock	188.33	23.80		3.95	2.24	0.05	1.64	2.92	9.34	13.85
1/4	48		Dark gray mudrock	197.71	75.62		3.06	1.51	0.14	1.57	1.61	8.82	13.40
1/5	54	Alov	Dark gray mudrock	186.96	34.59		3.73	2.67	0.18	1.66	1.70	9.33	14.73
1/6	57		Dark gray mudrock	247.65	39.46	10.63	3.61	1.20	0.08	1.64	2.07	9.67	12.56
1/7	67		Dark gray mudrock	216.17	79.38	10.38	4.19	1.00	0.26	1.71	2.16	11.10	18.34
1/8	73		Dark gray mudrock	229.55	59.40	10.42	5.81	0.68	0.08	1.75	1.76	12.43	18.84
1/9	76		Dark gray mudrock	196.27	73.62	17.47	4.93	0.52	0.12	1.52	2.52	11.37	18.55
1/10	85	Zarykley	Dark gray mudrock	140.59	39.93	12.23	4.70	0.35	0.13	1.41	1.97	9.38	17.19
1/11	91		Dark gray mudrock	262.77	65.85	19.83	5.10	0.98	0.15	1.78	2.59	13.27	19.65
1/12	94		Dark gray mudrock	261.76	68.81	34.99	5.24	1.83	0.22	1.57	3.03	12.51	17.19
1/13	100	Studenets	Dark gray mudrock	185.00	63.75	23.37	3.93	5.72	0.34	1.83	4.95	11.18	15.48
1/14	105		Brownish-gray black shale	68.83	36.99	27.34	1.02	99.35	2.04	0.36	6.56	2.53	3.75
1/14a	106		Brownish-gray black shale	309.07	119.81	25.97	16.76	102.96	2.13	1.08	12.93	8.69	
1/15	107		Gray marlstone	80.74	38.36	7.00	0.00	53.04	0.46	0.41	8.22	2.08	3.42
1/16	107.8	Ulyanovsk	Brownish-gray black shale	304.88	133.92	24.95	4.39	111.89	2.48	1.33	12.34	9.08	12.80
1/16a	108		Brownish-gray black shale	263.40	136.10	27.64	4.26	106.49	8.74	1.24	15.24	9.73	11.12
1/17	109		Dark gray mudrock	328.99	144.37	28.92	3.75	147.34	5.35	1.95	21.18	10.28	12.87
1/18	115	Khmelev	Dark gray mudrock	199.69	66.56	16.10	4.98	2.38	0.11	2.04	2.59	13.08	18.14
1/19	120		Dark gray mudrock	210.85	60.82	8.27	4.95	1.55	0.13	1.75	2.39	13.38	18.30
1/20	130		Dark gray mudrock	205.56	66.97	18.24	5.36	0.78	0.22	1.58	2.31	12.56	16.43
1/21	138		Greenish-gray siltstone	155.66	26.24	11.76	4.07	0.46	0.07	0.87	1.47	8.70	15.14
1/22	148	Uren	Dark gray mudrock	158.52	52.25	9.66	3.65	0.42	0.13	1.67	2.05	10.67	17.35
1/23	180		Dark gray mudrock	254.96	66.46	14.29	5.20	1.04	0.13	1.86	2.30	11.67	17.92
1/24	190	Klimov	Dark gray mudrock	267.99	48.02	26.06	2.44	1.91	0.11	1.99	2.35	11.90	17.63
1/25	220		Dark gray mudrock	201.45	59.37	21.80	3.91	0.58	0.63	1.62	2.65	13.44	17.67
1/26	240	Promzino	Brownish-gray black shale	141.68	159.47	20.14	3.18	22.48	1.79	0.75	13.16	6.20	6.72
1/27	241		Brownish-gray black shale	142.82	137.06	28.77	3.42	24.17	2.21	0.72	14.09	6.59	7.45
1/29	257	Trazov	Bluish-gray marlstone	120.71	228.37	9.39	3.41	3.19	0.83	1.24	5.08	10.17	9.66
1/30	293	Novikov	Bluish-gray marlstone	158.49	109.69	11.37	3.52	1.80	0.13	2.16	3.12	13.05	13.20

Table 3. Estimated redox proxies for the Upper Jurassic–Lower Cretaceous rocks from the Tatar-Shatrashany section. Gray intervals correspond to black shales.

Sample	Mo (ppm)	Mo/TOC (ppm/%)	U/Th (ppm/ppm)	U _{au}	V/Al (ppm/%)	U/Al (ppm/%)	Mo/Al (ppm/%)	TOC/P _{tot} (%/%)
1/3	2.2	1.7	0.3	-0.2	25.7	0.4	0.3	38.7
1/4	1.5	0.9	0.2	-1.3	27.9	0.2	0.2	72.2
1/5	2.7	1.6	0.2	-1.4	24.0	0.2	0.3	18.3
1/6	1.2	0.8	0.2	-1.2	37.3	0.3	0.2	7.4
1/7	1.0	0.7	0.2	-1.5	22.3	0.2	0.1	16.5
1/8	0.7	0.4	0.1	-2.4	23.0	0.2	0.1	26.2
1/9	0.5	0.4	0.2	-1.3	20.0	0.3	0.1	17.1
1/10	0.4	0.4	0.2	-1.2	15.4	0.2	0.0	9.7
1/11	1.0	0.7	0.2	-1.8	25.3	0.2	0.1	25.6
1/12	1.8	1.1	0.2	-1.1	28.8	0.3	0.2	31.5
1/13	5.7	2.2	0.4	1.2	22.6	0.6	0.7	11.7
1/14	99.4	15.4	2.6	5.7	34.7	3.3	50.0	50.1
1/14a	103.0	10.3	1.5	10.0				
1/15	53.0	41.6	4.0	7.5	44.6	4.5	29.3	26.5
1/16	111.9	14.8	1.4	9.3	45.0	1.8	16.5	125.0
1/16a	106.5	14.4	1.6	12.0	44.7	2.6	18.1	35.8
1/17	147.3	24.2	2.1	17.8	48.3	3.1	21.6	28.9
1/18	2.4	2.4	0.2	-1.8	20.8	0.3	0.2	3.6
1/19	1.6	1.4	0.2	-2.1	21.8	0.2	0.2	11.5
1/20	0.8	0.8	0.2	-1.9	23.6	0.3	0.1	16.3
1/21	0.5	1.5	0.2	-1.4	19.4	0.2	0.1	3.7
1/22	0.4	0.5	0.2	-1.5	17.3	0.2	0.0	10.2
1/23	1.0	0.8	0.2	-1.6	26.9	0.2	0.1	22.2
1/24	1.9	1.5	0.2	-1.6	28.7	0.3	0.2	40.6
1/25	4.0	3.1	0.5	2.8	25.3	0.8	0.4	50.5
1/26	22.5	0.8	2.1	11.1	39.8	3.7	6.3	112.2
1/27	24.2	2.9	2.1	11.9	36.2	3.6	6.1	74.6
1/29	3.2	9.1	0.5	1.7	23.6	1.0	0.6	2.2
1/30	1.8	3.0	0.2	-1.2	22.7	0.4	0.3	13.9

Pyrite framboid distributions are shown in Table 4 and their size is plotted in the graphic log (Fig. 4). The samples from the Lower Aptian OAE-1a reveal mean diameters of pyrite framboids between 6.8 μm and 8.1 μm and standard deviation 1.7–2.2 μm . Whereas, pyrite framboids found in the Middle Volgian black shales display higher mean diameters (7.2–7.9 μm) and standard deviation (2.8–3.0 μm).

Geoaccumulation index

The obtained I_{geo} values revealed that all the samples from the organic carbon-poor host rocks fell within the uncontaminated to moderately contaminated categories by Pb, Zn, Ni, Cu, and V (Tab. 5, Fig. 5). But, the Middle Volgian Promzino black shales fell within the

Table 4. Pyrite framboid distributions in the upper Middle Volgian and Lower Aptian black shales from the Tatar-Shatrashany section.

Substage	Formation	Sample	Lithology	Number of framboids	Framboid diameter (μm)				Redox conditions
					Max	Min	Mean	Standard deviation	
Lower Aptian	Ulyanovsk	1/14	Black shales	38	8.6	7.9	8.1	1.7	Anoxic
		1/16	Black shales	47	8.2	7.4	7.6	1.8	Anoxic
		1/17	Black shales	55	7.1	6.2	6.8	2.2	Anoxic
Middle Volgian	Promzino	1/26	Oil shales	25	9.4	6.5	7.2	2.0	Anoxic
		1/27	Black shales	32	8.6	6.8	7.9	3.8	Dysoxic
		1/27a	Black shales	23	9.7	7.3	7.8	3.0	Dysoxic

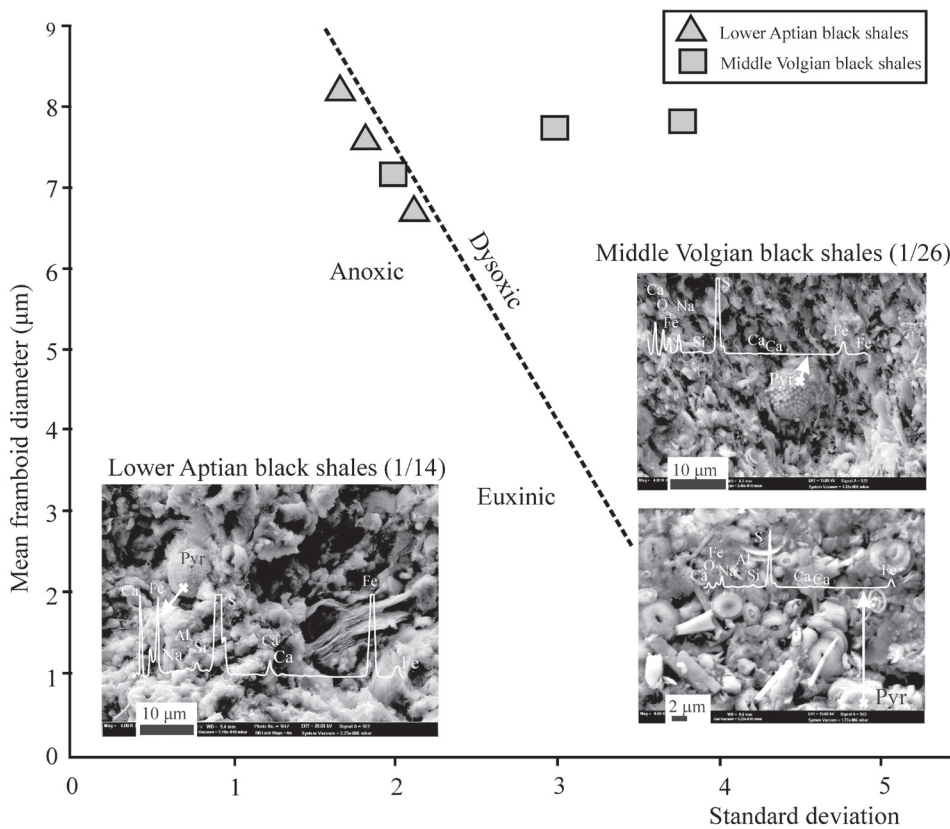


Figure 4. Mean versus standard deviation plot of pyrite framboid data from the Lower Aptian and Middle Volgian black shales of the Tatar-Shatrashany section (Bond & Wignall 2010). SEM images and EDS of close-packed (samples 1/14 and 1/26) and disintegrated (sample 1/26) pyrite framboid.

heavily to extremely contaminated categories by Cd and Mo (samples 1/26 and 1/27), while the Lower Aptian black shales (samples 1/14–1/17) showed the extreme contamination by Cd and Mo as well (Fig. 5).

Benthic foraminiferal diversity and abundance

A rich complex of benthic foraminifers was found in the study section (Zorina & Startseva 2010) for which a total number of specimens (per 1 m²) and a number of species

in the sample are counted (Tab. 6, Fig. 5). The highest number of specimens and number of species (5680 and 14, respectively) occur in the organic carbon-poor Novikov marls and Klimov–Uren mudrocks (1400–3240 and 3–9, respectively). The Promzino and Ulyanovsk black shales show considerable low values of these two parameters varying for the number of specimens in the 0–1400 and 0–520 ranges, respectively, and for the number of species in the 0–5 and 0–1 ranges, respectively. Noteworthy, most samples from the Ulyanovsk formation contain no benthic foraminifers.

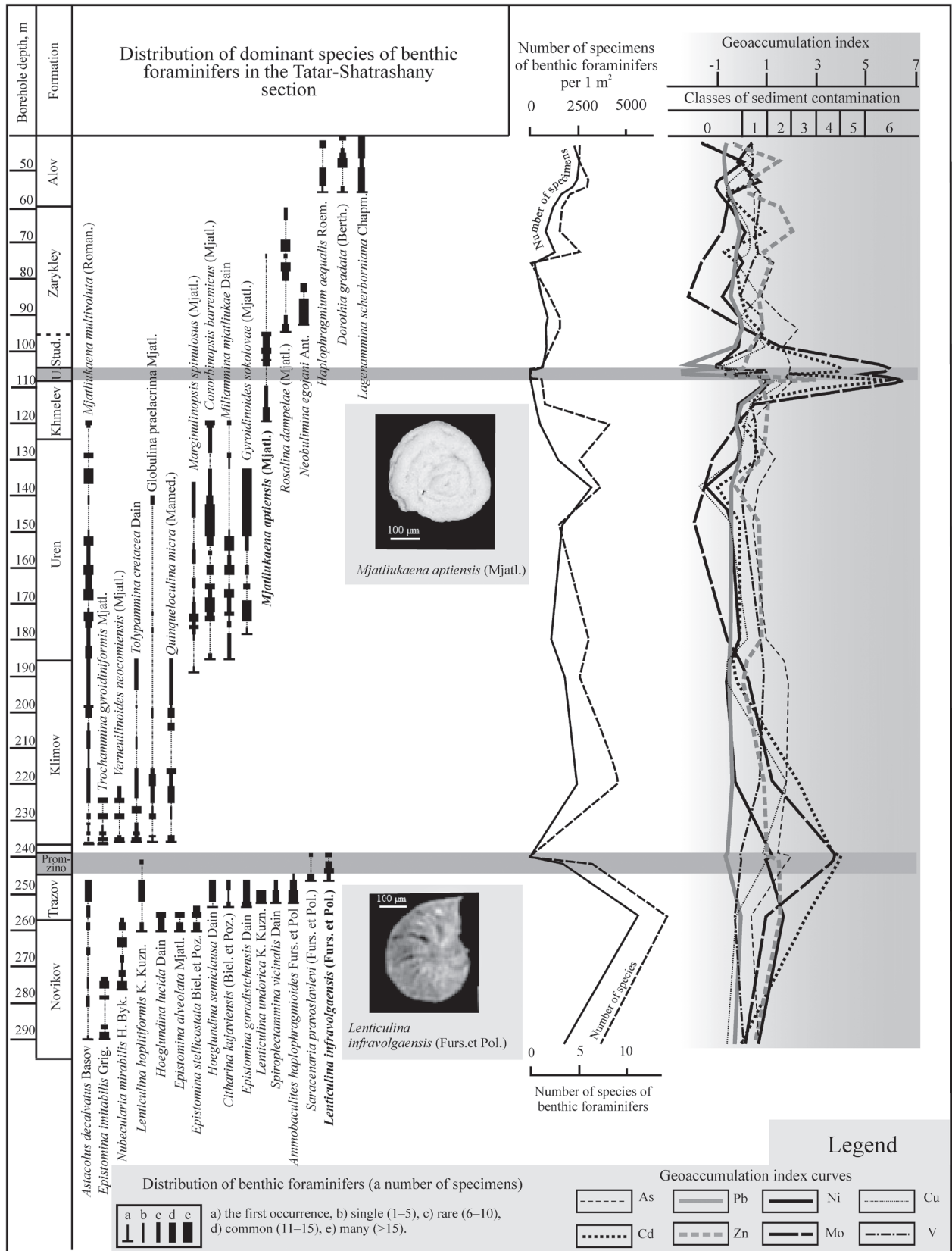


Figure 5. Distribution of dominant species of benthic foraminifers in the Upper Jurassic–Lower Cretaceous strata of the Tatar-Shatrashany borehole (modified from Zorina & Startseva 2010), foraminiferal abundance and diversity curves, and the I_{geo} curves for toxic metals.

Table 5. Index I_{geo} values for studied samples from the Tatar-Shatrashany section. Gray areas correspond to black shales.

Sample	As	Cd	Pb	Zn	Ni	Mo	Cu	V	W
1/3	–	–1.58	–0.65	–0.24	–1.57	0.44	–0.30	0.37	–0.80
1/4	–	0.08	–0.65	1.51	0.10	–0.12	0.51	0.44	–0.86
1/5	–	0.38	–0.72	0.16	–1.03	0.69	–0.55	0.36	–0.78
1/6	0.56	–0.67	–0.45	1.01	–0.84	–0.46	–0.57	0.77	–0.80
1/7	0.53	0.92	–0.10	2.13	0.17	–0.72	0.27	0.57	–0.73
1/8	0.53	–0.74	–0.22	0.85	–0.25	–1.28	0.28	0.66	–0.70
1/9	1.28	–0.17	–0.20	1.21	0.06	–1.66	–0.19	0.43	–0.90
1/10	0.76	–0.04	–0.53	0.67	–0.82	–2.22	0.70	–0.05	–1.01
1/11	1.46	0.18	–0.01	0.78	–0.10	–0.76	–0.02	0.85	–0.68
1/12	2.28	0.68	–0.10	0.86	–0.04	0.15	0.36	0.85	–0.86
1/13	1.70	1.32	–0.13	0.36	–0.15	1.79	0.93	0.35	–0.64
1/14	1.92	3.92	–2.30	0.08	–0.93	5.91	–0.80	–1.08	–2.99
1/14a	1.85	3.98	–0.50	0.08	0.77	5.96	0.85	1.09	–1.41
1/15	–0.04	1.78	–2.53	–0.52	–0.88	5.01	–0.66	–0.85	–2.80
1/16	1.79	4.20	–0.40	0.26	0.93	6.08	1.00	1.07	–1.10
1/16a	1.94	6.02	–0.37	3.18	0.95	6.01	0.89	0.86	–1.20
1/17	2.01	5.31	1.15	0.78	1.03	6.48	1.69	1.18	–0.55
1/18	1.16	–0.28	0.11	1.08	–0.08	0.53	0.37	0.46	–0.48
1/19	0.20	–0.06	–0.23	0.98	–0.21	–0.09	0.14	0.54	–0.70
1/20	1.34	0.73	–0.07	0.82	–0.07	–1.09	–0.11	0.50	–0.85
1/21	0.71	–0.99	–0.42	–0.24	–1.43	–1.83	–1.72	0.10	–1.71
1/22	0.42	–0.09	–0.40	0.68	–0.43	–1.96	–0.45	0.12	–0.77
1/23	0.99	–0.06	–0.40	0.77	–0.09	–0.67	0.23	0.81	–0.62
1/24	1.86	–0.32	–0.54	0.07	–0.55	0.21	–0.70	0.88	–0.52
1/25	1.60	2.22	–0.45	0.67	–0.25	–1.51	0.26	0.47	–0.81
1/26	1.48	3.73	–0.52	1.02	1.18	3.77	0.81	–0.04	–1.93
1/27	2.00	4.03	–0.69	1.48	0.96	3.87	1.13	–0.03	–1.99
1/29	0.38	2.62	–0.07	1.60	1.70	0.95	–0.24	–0.27	–1.20
1/30	0.66	–0.08	–0.29	0.50	0.64	0.12	–0.60	0.12	–0.40

Discussion

Trace elements as indicators of redox conditions

As anoxic basins are widely thought to act as traps for stable sulphide-forming trace elements (*e.g.*, Jacobs *et al.* 1985), specific elements must be located within the sediments rather than in the water column (Emerson & Huested 1991). Several trace elements such as Mo, Cr, V,

U, *etc.*, are enriched in reducing sediments and are highly sensitive to redox changes, making them important proxies for paleo-redox reconstruction (Calvert & Pedersen 1993, Jones & Manning 1994, Crusius *et al.* 1996, Helz *et al.* 1996, Algeo & Maynard 2004).

U is stable in form of insoluble U^{4+} under highly reducing conditions, which leads to the U enrichment in sediments, whereas it exists as soluble U^{6+} under oxidizing conditions, leading to the U release from sediments (Wignall & Twitchett 1996, Guo *et al.* 2007). The U/Th

Table 6. Quantitative data on abundance and diversity of benthic foraminifers from the Upper Jurassic–Lower Cretaceous rocks of the Tatar-Shatrashany section.

Samples	Stage/ Substage	Formation	Number of specimens per 100 gr	Number of specimens per 1m ²	Number of species
1/3			58	2320	5
1/4	Mid Albian	Alov	63	2520	5
1/5			57	2280	6
1/6			37	1480	4
1/7			19	760	3
1/8			32	1280	5
1/9	Mid Aptian	Zarykley	0	0	0
1/10			16	640	2
1/11			24	960	3
1/12			19	760	3
1/13		Studentets	21	840	2
1/14			13	520	1
1/14a			0	0	0
1/15	Lower Aptian	Ulyanovsk	0	0	0
1/16			0	0	0
1/16a			0	0	0
1/17			3	120	1
1/18		Khmelev	8	320	1
1/19			13	520	8
1/20			35	1400	5
1/21	Barremian	Uren	81	3240	7
1/22			44	1760	3
1/23			28	1120	6
1/24	Uper Hauterivian	Klimov	45	1800	5
1/25			61	2440	9
1/26	Middle Volgian	Promzino	0	0	0
1/27			35	1400	5
1/29	Lower Volgian	Trazov	142	5680	14
1/30	Upper Kimmeridgian	Novikov	41	1640	7

ratio has also been used as an indicator of redox conditions due to the different behavior of U and Th in terms of solubility (Rimmer *et al.* 2004). In contrast to U, Th is known to be a highly reactive-particle element being practically associated with clay minerals, insoluble debris, or heavy metals (Anderson *et al.* 1983). A ratio of U/Th higher than 1.25 marks an anoxic environment, and 0.75–1.25 signals a suboxic to dysoxic environment, while a ratio less than 0.75 indicates an oxic environment (Jones & Manning 1994). In accordance with these assumptions,

the Promzino and Ulyanovsk black shales are deposited in reducing environments of good preservation, while the host marls and mudrocks are deposited in the oxic conditions (Tab. 3, Fig. 3).

Wignall & Myers (1988) proposed the authigenic uranium content as an index of bottom water anoxia in ancient sedimentary sequences. The U_{au} content higher than 12.0 indicates anoxic conditions and 5.0–12.0 indicates suboxic to dysoxic conditions, while the U_{au} content lower than 5.0 indicates oxic conditions (Jones & Manning

1994). Our results mark mostly oxic conditions in which the host mudrocks are deposited. The Promzino black shales are formed in strongly dysoxic conditions, while the Ulyanovsk bituminous strata are deposited in the mostly dysoxic to euxinic conditions (Tab. 3, Fig. 3).

As trace element concentrations of marine sediment represent mixtures of both detrital and authigenic components, it is only the concentrations of authigenic components that vary in response to redox changes in the water column (Jiang *et al.* 2007). In order to minimize the effects of weathering and post-depositional alteration, it is customary to normalize trace element concentrations to Al contents (Tribovillard *et al.* 2006). The Promzino and Ulyanovsk black shales show distinctly high V/Al, U/Al, and Mo/Al ratios indicating reducing conditions, whereas organic carbon-poor strata show low values of these ratios marking oxic conditions in the basin (Tab. 3, Fig. 3).

Many researchers advocate the use of the TOC/P ratio as a robust proxy for productivity and bottom-water redox conditions (Tribovillard *et al.* 2006, Algeo & Ingall 2007, Westermann *et al.* 2013). Increased levels of organic matter burial under anoxic bottom result in simultaneous remobilization and escape of phosphorus from sediment into the water. Studies of modern marine environments suggest that the TOC/P ratio of sediment that is deposited under permanently anoxic conditions is >150 whereas sediment that accumulated under oxic bottom-water conditions is characterized by TOC/P < 30. Intermediate values indicate dysoxic conditions (Algeo & Ingall 2007). Elevated TOC/P ratios in the organic carbon-rich Promzino and Ulyanovsk Fms display that the strata were deposited under unstable oxic to anoxic conditions whereas the host mudrocks were formed mostly in oxic-dysoxic conditions (Tab. 3, Fig. 3).

Pyrite framboids as indicators of redox conditions

Pyrite framboids are well known as raspberry-shaped, spherical aggregates (2–50 µm in diameter) consisting of cubo-octahedral to octahedral, equimorphic microcrystals (0.5–2 µm) (Park *et al.* 2003, Cavalazzi *et al.* 2014). Pyrite framboids are very common in black shales being formed in weakly reducing euxinic conditions as syndimentary precipitates due to bacterially driven iron- and sulfate-reduction (Wignall *et al.* 2005, Oschmann 2011, Cavalazzi *et al.* 2014).

There is no agreement on the origin of pyrite framboids, probably because they could be formed under different environmental conditions. It has been assumed that magnetotactic bacteria could contain ferromagnetic sulphides (Taylor 1983, Sawlowicz 1993). Farina

et al. (1990) showed that a colony of magnetotactic bacteria is similar to framboids in appearance and size (5–10 µm).

As homogenization of framboids usually spreads from the centre to the surface of the spherules, organic matter and clay particles may be captured as inclusions (Sawlowicz 1993). The dense packing of the pyrite microgranules enveloping the organic matter in these framboids suggests a euxinic environment in the basin (Wang *et al.* 2012). Thus, it would be appropriate to assume euxinia in the basin, a condition in which hydrogen sulphide concentrations increase to toxic levels (Meyer & Kump 2008). Close-packed framboids found in both Promzino and Ulyanovsk black shales (Fig. 4) point to the strong deficiency of oxygen in the study basin during the Late Jurassic and Early Aptian OAEs (Zorina *et al.* 2017). But, disintegrating framboids identified in Promzino black shales (Fig. 4) indicate partial or complete dissolution of the organic matter inside the framboids, which resulted in their decay. In conjunction with the abundant faunal remains, this likely indicates an increasing water oxygenation.

It has been established that abundant pyrite framboids can be found in areas of oxygen deficiency (dysoxic and anoxic conditions) and hydrogen sulphide contamination (euxinic conditions). In a basin with euxinia, due to the high density of framboids, their sizes remain uniformly small and do not vary over a wide range, whereas under conditions of insignificant oxidization, the diameters of framboids can differ markedly, while the standard deviation of their diameters is much larger than those formed under euxinic conditions (Bond & Wignall 2010). Consequently, the dependence of the mean diameters of framboids on their standard deviation makes it possible to reveal the distribution of framboids over the indicated areas on the Bond-Wignall diagram and to determine redox conditions in the basin (Wilkin *et al.* 1996, Wilkin & Barnes 1997, Wignall *et al.* 2010).

The mean diameter versus standard deviation plot indicates anoxic or dysoxic depositional environments for studied organic carbon-rich levels. So, the samples from the Lower Aptian OAE-1a-related black shales plot within the field of anoxic conditions, whereas, samples from the Middle Volgian black shales plot within the fields of both dysoxic and anoxic conditions (Fig. 4). This could evidence for mutative conditions under which minor oxidation alternated with periods of anoxia.

Benthic foraminiferal response to toxic metal contamination

Benthic foraminifera from recent basins have been successfully used as proxies for studying the impact of

some pollutants, including heavy metals, chemicals, and oil, as well as thermal and organic contaminants. The development of test abnormalities is suitable for investigating the response of benthic foraminifers to stress including pollution (Yanko *et al.* 1999, Frontalini *et al.* 2009, Geslin *et al.* 1998). No malformations in the community of benthic foraminifers that could point to the toxicity of sediments were observed.

The response of benthic foraminifers to TM contamination in the sea basins of the geological past is poorly discussed in scientific reports, but it is well observed for recent basins. As assemblages of benthic foraminifers are known to be continuously exposed to variable concentrations of TM in seawater (Begum 2012), they suffer a declining diversity as a response to TM pollution (Debenay & Fernandez 2009). The lowest foraminiferal diversity was found in the muddy sediments with high concentration of Cu, Zn, Pb, Cd, Hg, Cr, Ni, As, Rb, Br, and some others (Alve 1991, Alyazichi *et al.* 2014, Murray 2006, Caruso *et al.* 2011).

The calculated parameters of abundance and diversity of benthic foraminifers in the study section are generally correlated with each other, and their variation shows that the communities of benthic foraminifers were numerous and diverse in the Late Jurassic–Early Cretaceous, except for the Late Jurassic and Early Cretaceous anoxic episodes (Fig. 5).

As buried foraminiferal assemblages represent the product of both subtle environmental changes and post-depositional modifications (Olszewski 2004, Berkeley 2009), low foraminiferal abundance and diversity could be caused by postpositional taphonomic effects. The effect of dissolution of foraminifers is well-known (Murray 1989, Murray & Alve 1999). Assemblages may experience compositional changes due to selective taphonomic loss during burial. Berkeley (2009) assumed that it could be caused by relative sea-level changes. Although this approach explains well recurring selective taphonomic losses in foraminiferal assemblages observed in the geological past, it can be applied mostly to modern sediments accumulating in narrowly constrained zones at specific positions relative to the tide (Berkeley 2009). Thus, the observed decrease in foraminiferal abundance and diversity was probably not caused by the aforementioned post-depositional taphonomic effects but more likely by anoxic conditions and in particular, by TM contamination of sediments in which the foraminifers are buried.

In the Promzino black shales, five species of benthic foraminifers, including the zonal species *Lenticulina infravolgaensis* (Furs. et Pol.) are found only in few samples (Fig. 5). In most of Promzino sediment samples, the I_{geo} index indicates significant contamination by Cd and Mo.

On the contrary, benthic foraminifers are not found, and only a few specimens of the species *Mjatliukaena aptiensis* (Mjatl.) are identified at the lower and upper layers of the Ulyanovsk black shales (Fig. 5). At the same time, the concentrations of Cd and Mo in rocks are extremely high, and according to the index I_{geo} values, the sediments could be classified as extremely contaminated by Mo and moderately to extremely contaminated by Cd.

The effects of metal toxicity are known for some extant nannoplankton species. For example, cadmium inhibits calcification and copper is not tolerated by several coccolithophorid species (Brand 1994). In the Cretaceous, *Biscutum* suffered the presence of toxic metals introduced in large quantities via hydrothermal plumes (Erba 2004). Similar enrichment in Mo and some other toxic elements are reported to be observed in Lower Cambrian black shales in southern China (Pořavič *et al.* 2006).

To sum up, the integrated data provide an evidence for mostly dysoxic conditions in the North-Eastern Peri Tethys during the Late Jurassic anoxic event, during which the habitat conditions were not destructive for benthic foraminifers. The most toxic-resistant species was *Lenticulina infravolgaensis* (Furs. et Pol.).

Strong anoxia in Early Aptian OAE 1a that contributed to the extremely contaminated sediments is considered to have been fatal for benthic foraminifers. The most toxic-resistant species was the zonal species *Mjatliukaena aptiensis* (Mjatl.).

Modeling paleoenvironments in the North-Eastern Peri-Tethys in Early Aptian

Since OAEs are interpreted as a concatenation of sedimentary, geochemical, and biological events (Jenkyns 2010), the Late Jurassic and the Early Aptian OAEs may cause and record massive climate, sea-level, and environmental changes in the epeiric basin of the North-Eastern Peri-Tethys. The most dramatic changes in depositional environments are found to take place during the Early Aptian OAE-1a which is shown in the paleoenvironmental models presented (Fig. 6). The latest Barremian–earliest Aptian (pre-event) conditions were favorable for nektonic inhabitants such as ammonites and belemnites due to normal oxygen circulation and seawater temperatures ranging between 7 and 18 °C (Zakharov *et al.* 2013) (Fig. 6A). During this period, the bioturbated dark gray mudrocks with a significant contribution of terrigenous mud, silt, and pyroclastic material accumulated at an estimated depth of around 200 m (Zorina 2009, 2014, 2019; Zorina *et al.* 2020). Element geochemistry of the mudrocks confirms uncontaminated oxic conditions (Figs 3, 5), which were suitable for benthic foraminifers and the activity of burrowing organisms.

Accompanied by global warming and eustatic high-stand (Haq 2014) the OAE 1a has been manifested in the studied region by a rise in a seafloor temperature to

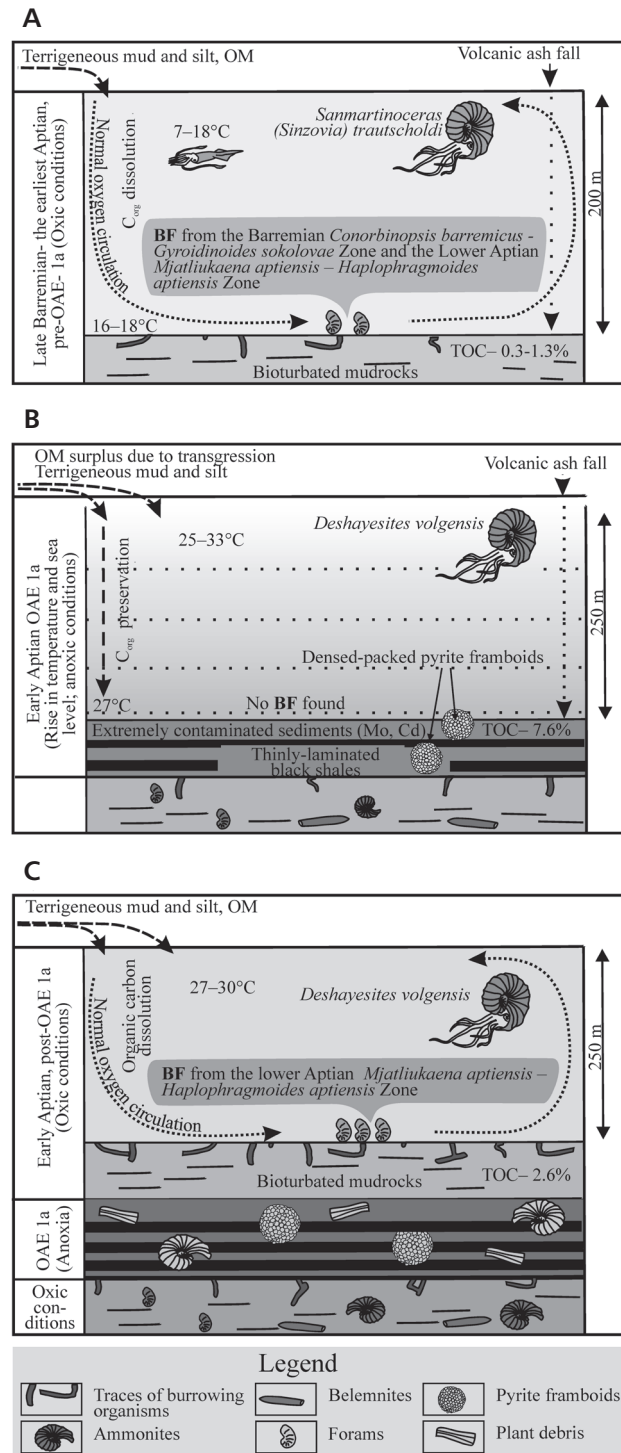


Figure 6. Models to illustrate the variety of biotic and abiotic processes characteristic of the pre-OAE 1a (A), OAE 1a (B), post-OAE 1a (C) in the North-Eastern Peri-Tethys. Temperature is given after (Zakharov *et al.* 2013). Abbreviations: BF– benthic foraminifers; OM – organic matter. For Lithology, see Legend in Fig. 2.

25–33 °C (Zakharov *et al.* 2013), the 3rd order transgression (Zorina 2016), and basin depth increase to 250 m (Zorina 2014, 2019) (Fig. 6 b). Normal oxygenated water circulation was changed by “sluggish” water stagnation which has led to the deposition of laminated strata, organic matter burial, formation of close-packed pyrite framboids, and a spread of anoxia in the bottom part of the basin (Fig. 6B). The latest is evidenced by the elevated values of redox-sensitive elements and their ratios, and pyrite framboids diameter measurements (Figs 3–5). The Lower Aptian black shales showed extreme contamination by Mo and Cd, thus the anoxic environment became unsuitable for the life of benthic foraminifers due to the combined effects of oxygen deficiency, possible excess of free hydrogen sulphide, and elevated concentrations of toxic metals.

The post-OAE 1a conditions are proposed to record a recovery phase during which normal water circulation was recovered (Fig. 6C). During this phase, the seawater temperatures varied between 27 and 30 °C (Zakharov *et al.* 2013), water depth was estimated to be at about 250 m (Zorina 2014, 2019), and bioturbated uncontaminated dark gray mudrocks with TOC value of 2.6% accumulated. The toxic and disastrous consequences of the OAE 1a anoxia terminated and more suitable conditions for benthic foraminifers from the Lower Aptian *Mjatliukaena aptiensis*-*Haplophragmoides aptiensis* Zone were restored directly above the black shales, including the only toxic-resistant species *Mjatliukaena aptiensis* (Mjatl.) (Fig. 5).

Conclusions

Reducing conditions are identified and toxic environments reconstructed during the OAE 1a in the deepening and transgressing epeiric basin in the North-Eastern Peri-Tethys.

Extreme contamination of the OAE 1a-related black shales by Mo and Cd in conjunction with the absence of oxygen could result in conditions not suitable for benthic foraminifers dwelling. The key species *Mjatliukaena aptiensis* (Mjatl.) is regarded to be one of the toxic-resistant species that successfully recovered from the OAE 1a anoxic stress.

Comparing to the Late Jurassic OAE, the integrated data indicate moderately contaminated black shales and mainly dysoxic conditions under which habitat conditions were not completely detrimental for benthic foraminifers. The most toxic-resistant species was *Lenticulina infravolgensis* (Furs. et Pol.).

The paleoenvironment models integrated biotic and abiotic data may help to better understand modern climate changes.

Acknowledgments

The author thanks Tomáš Kumpan, Ondřej Bábek, and the anonymous reviewer for their critical comments and useful suggestions to improve the manuscript. N.V. Sokerina and B.I. Gareev are acknowledged for their help with providing analyses. This work was supported by the Ministry of Science and Higher Education of the Russian Federation under agreement No. 075-15-2020-931 within the framework of the development program for a world-class Research Center “Efficient development of the global liquid hydrocarbon reserves”.

References

- ALGEO, T.J. & INGALL, E. 2007. Sedimentary C_{org} : P ratios, paleocean ventilation, and Phanerozoic atmospheric pO_2 . *Palaeogeography, Palaeoclimatology, Palaeoecology* 256, 130–155. DOI 10.1016/j.palaeo.2007.02.029
- ALGEO, T.J. & MAYNARD, J.B. 2004. Trace-element behavior and redox facies in core shales of Upper Pennsylvanian Kansas-type cyclothems. *Chemical Geology* 206, 289–318. DOI 10.1016/j.chemgeo.2003.12.009
- ALVE, E. 1991. Benthic foraminifera in sediment cores reflecting heavy metal pollution in Sorfjord, western Norway. *Journal of Foraminiferal Research* 21(1), 1–19. DOI 10.2113/gsjfr.21.1.1
- ALYAZICHI, Y.M., JONES, B. & MCLEAN, E. 2014. Environmental assessment of benthic foraminiferal and pollution in Gunnammatta Bay, NSW, Australia, 2495–2504. In SHIMIZU, N., KANEKO, K. & KODAMA, J. (eds) *Rock Mechanics for Global Issues – Natural Disasters, Environment, and Energy. Proceedings of the 2014 ISRM International Symposium*.
- ANDERSON, R.F., BACON, M.P. & BREWER, P.G. 1983. Removal of ^{230}Th and ^{231}Pa at ocean margins. *Earth and Planetary Science Letters* 66, 73–90. DOI 10.1016/0012-821X(83)90127-9
- ATKINSON, W.J. 1967. *Regional geochemical studies in county Limerick, Ireland with particular reference to selenium and molybdenum*. 337 pp. Ph.D. thesis, Imperial College, London.
- BEGUM, G. (ed.) 2012. *Ecotoxicology*. 146 pp. InTech, Croatia. DOI 10.5772/1185
- BERKELEY, A. 2009. Understanding the role of taphonomy and post-depositional processes on the intertidal stratigraphic record. *Palaios* 24, 271–272. DOI 10.2110/palo.2009.S03
- BOND, D.P.G. & WIGNALL, P.B. 2010. Pyrite framboid study of marine Permian-Triassic boundary sections: A complex anoxic event and its relationship to contemporaneous mass extinction. *GSA Bulletin* 122(7/8), 1265–1279. DOI 10.1130/B30042.1
- BOTTINI, C., ERBA, E., TIRABOSCHI, D., JENKYN, H.C., SCHOUTEN, S. & SINNINGHE DAMSTÉ, J.S. 2015. Climate variability and ocean fertility during the Aptian Stage. *Climate Past* 11, 383–402. DOI 10.5194/cp-11-383-2015
- BRAND, L.E. 1994. Physiological ecology of marine coccolithophores, 39–49. In WINTER, A. & SIESSER, W.G. (eds) *Coccolithophores*. Cambridge University Press, Cambridge.
- CAVALAZZI, B., AGANGI, A., BARBIERI, R., FRANCHI, F. & GASPAROTTO, G. 2014. The Formation of Low-Temperature Sedimentary Pyrite and Its Relationship with Biologically-Induced Processes. *Geology of Oil Deposits* 56, 395–408. DOI 10.1134/S107570151405002X
- CALVERT, S.E. & PEDERSEN, T.F. 1993. Geochemistry of recent oxic and anoxic marine sediments: implications for the geological record. *Marine Geology* 113, 67–88. DOI 10.1016/0025-3227(93)90150-T
- CARUSO, A., COSENTINO, C., TRANCHINA, L. & BRAI, M. 2011. Response of benthic foraminifera to heavy metal contamination in marine sediments (Sicilian coasts, Mediterranean Sea). *Chemistry and Ecology* 27(1), 9–30. DOI 10.1080/02757540.2010.529076
- CRUSIUS, J., CALVERT, S., PEDERSEN, T. & SAGE, D. 1996. Rhenium and molybdenum enrichments in sediments as indicators of oxic, suboxic, and sulfidic conditions of deposition. *Earth and Planetary Science Letters* 145, 65–78. DOI 10.1016/S0012-821X(96)00204-X
- DEAN, W.E., GARDNER, J.V. & PIPER, D.Z. 1997. Inorganic geochemical indicators of glacial-interglacial changes in productivity and anoxia on the California continental margin. *Geochimica et Cosmochimica Acta* 61, 4507–4518. DOI 10.1016/S0016-7037(97)00237-8
- DEBENAY, J.-P. & FERNANDEZ, J.-M. 2009. Benthic foraminifera records of complex anthropogenic environmental changes combined with geochemical data in a tropical bay of New Caledonia (SW Pacific). *Marine Pollution Bulletin* 59, 311–322. DOI 10.1016/j.marpolbul.2009.09.014
- EMERSON, S.R. & HUESTED, S.S. 1991. Ocean anoxia and the concentrations of molybdenum and vanadium in seawater. *Marine Chemistry* 34, 177–196. DOI 10.1016/0304-4203(91)90002-E
- ERBA, E. 2004. Calcareous nannofossils and Mesozoic oceanic anoxic events. *Marine Micropaleontology* 52, 85–106. DOI 10.1016/j.marmicro.2004.04.007
- ERBA, E., BOTTINI, C., WEISSERT, J.H. & KELLER, C.E., 2010. Calcareous Nannoplankton Response to Surface-Water Acidification Around Oceanic Anoxic Event 1a. *Science* 329, 428–432. DOI 10.1126/science.1188886
- FARINA, F., ESQUIVEL, D.M.S. & LINS DE BARROS H.G.P. 1990. Magnetic iron-sulphur crystals from a magnetotactic microorganism. *Nature* 343, 256–258. DOI 10.1038/343256a0
- FRENCH, K.L., SEPÚLVEDA, J., TRABUCHO-ALEXANDRE, J., GRÖCKE, D.R. & SUMMONS, R.E. 2014. Organic geochemistry of the early Toarcian oceanic anoxic event in Hawsker Bottoms, Yorkshire, England. *Earth and Planetary Science Letters* 390, 116–127. DOI 10.1016/j.epsl.2013.12.033
- FRIEDRICH, O. 2010. Benthic foraminifera and their role to decipher paleoenvironment during mid-Cretaceous Oceanic Anoxic Events – the “anoxic benthic foraminifera” paradox. *Revue de micropaléontologie* 53, 175–192. DOI 10.1016/j.revmic.2009.06.001
- FRONTALINI, F., BUOSI, C., DA PELO, S., COCCIONI, R., CHERCHI, A. & BUCCI, C. 2009. Benthic Foraminifera as Bio-Indicators of Trace Element Pollution in the Heavily Contaminated Santa

- Gilla Lagoon (Cagliari, Italy). *Marine Pollution Bulletin* 58(6), 858–877. DOI 10.1016/j.marpolbul.2009.01.015
- GALIAKBEROV, A., ZORINA S., MAKSYUTOVA, L., DZHALLMUKHANOVA, R., ZARIPOVA, G. & NIKASHIN, K. 2018. Toxicity of high-carbon sediments: case Study from anoxic basins of the East European and West Siberian Platforms, 340–343. In NOURGALIEV, D.K. (ed.) *Advances in Devonian, Carboniferous, and Permian Research: Stratigraphy, Environments, Climate, and Resources. Filodiritto Editore–Proceedings*.
- GAVRILOV, YU.O., SHCHEPETOVA, E.V., BARABOSHKIN, E.YU. & SHCHERBININA, E.A. 2002. The Early Cretaceous anoxic basin of the Russian Plate: sedimentology and geochemistry. *Lithology and Mineral Resources* 37, 310–329. DOI 10.1023/A:1019943305677
- GESLIN, E., DEBENAY, J.P. & LESOURD, M. 1998. Abnormal wall textures and test deformation in Ammonia (Hyaline Foraminifer). *Journal of Foraminiferal Research* 28(2), 148–156.
- GUO, Q., SHIELDS, G.A., LIU, C., STRAUSS, H., ZHU, M., PI, D., GOLDBERG, T. & YANG, X. 2007. Trace element chemostratigraphy of two Ediacaran-Cambrian successions in South China: implications for organosedimentary metal enrichment and silicification in the Early Cambrian. *Palaeogeography, Palaeoclimatology, Palaeoecology* 254, 194–216. DOI 10.1016/j.palaeo.2007.03.016
- HAQ, B.U. 2014. Cretaceous eustasy revisited. *Global and Planetary Change* 113, 44–58. DOI 10.1016/j.gloplacha.2013.12.007
- HELZ, G.R., MILLER, C.V., CHARNOCK, J.M., MOSSELMANS, J.F.M., PATRICK, R.A.D., GARNER, C.D. & VAUGHAN, D.J. 1996. Mechanisms of molybdenum removal from the sea and its concentration in black shales: EXAFS evidence. *Geochimica et Cosmochimica Acta* 60, 3631–3642. DOI 10.1016/0016-7037(96)00195-0
- JACOBS, L., EMERSON, S. & SKEI, J. 1985. Partitioning and transport of metals across the O₂/H₂S interface in a permanently anoxic basin: Framvaren Fjord, Norway. *Geochimica et Cosmochimica Acta* 49, 1433–1444. DOI 10.1016/0016-7037(85)90293-5
- JAHREN, A.H., ARENS, N.C., SARMIENTO, G., GUERRERO, J. & AMUNDSON, R. 2001. Terrestrial record of methane hydrate dissociation in the Early Cretaceous. *Geology* 29, 159–162. DOI 10.1130/0091-7613(2001)029<0159:TROMHD>2.0.CO;2
- JENKYN, H.C. 2010. Geochemistry of oceanic anoxic events. *Geochemistry, Geophysics, Geosystems* 11(3), Q03004. DOI 10.1029/2009GC002788
- JIANG, S.Y., ZHAO, H.X., CHEN, Y.Q., YANG, T., YANG, J.H. & LING, H.F. 2007. Trace and rare earth element geochemistry of phosphate nodules from the lower Cambrian black shale sequence in the Mufu Mountain of Nanjing, Jiangsu province, China. *Chemical Geology* 244(3–4), 584–604. DOI 10.1016/j.chemgeo.2007.07.010
- JONES, B. & MANNING, D.A.C. 1994. Comparison of geochemical indices used for the interpretation of palaeoredox conditions in ancient mudstones. *Chemical Geology* 111, 111–129. DOI 10.1016/0009-2541(94)90085-X
- KELLER, C.E., HOCHULI, P.A., WEISSERT, H., BERNASCONI, S.M., GIORGIONI, M. & GARCIA, T.I. 2011. A volcanically induced climate warming and floral change preceded the onset of OAE1a (Early Cretaceous). *Palaeogeography, Palaeoclimatology, Palaeoecology* 305, 43–49. DOI 10.1016/j.palaeo.2011.02.011
- KETRIS, M.P. & YUDOVICH, Y.E. 2009. Estimation of clarkes for carbonaceous biolithes: world averages for trace elements contents in black shales and coals. *International Journal of Coal Geology* 78, 135–148. DOI 10.1016/j.coal.2009.01.002
- LARSON, R.L. & ERBA, E. 1999. Onset of the mid-Cretaceous greenhouse in the Barremian–Aptian: igneous events and the biological, sedimentary, and geochemical responses. *Paleoceanography* 14, 553–678. DOI 10.1029/1999PA900040
- LEE, J.-S., CHON, H.-T., KIM, J.-SH., KIM, K.-W. & MOON, H.-S. 1998. Enrichment of potentially toxic elements in areas underlain by black shales and slates in Korea. *Environmental Geochemistry and Health* 20, 135–147.
- LI, Y.X., BRALOWER, T.J., MONTANEZ, I.P., OSLEGER, D.A., ARTHUR, M.A., BICE, D.M., HERBERT, T.D., ERBA, E. & PREMOLI SILVA, I. 2008. Toward an orbital chronology for the early Aptian Oceanic Anoxic Event (OAE1a, ~120 Ma). *Earth and Planetary Science Letters* 271, 88–100. DOI 10.1016/j.epsl.2008.03.055
- LUND, L.J., BETTY, E.E., PAGE, A.L. & ELLIOTT, R.A. 1981. Occurrence of naturally high cadmium levels in soils and its accumulation by vegetation. *Journal of Environmental Quality* 10, 551–556. DOI 10.2134/jeq1981.00472425001000040027x
- MAKSYUTOVA, L.F., GALIAKBEROV, A.I., DZHALLMUKHANOVA, R.I., ZARIPOVA, G.M., NIKASHIN, K.I. & ZORINA, S.O. 2018. New data on greenhouse-gas footprint from black shales of Russian and West Siberian Platforms, Russia, 375–380. In NOURGALIEV, D.K. (ed.) *Advances in Devonian, Carboniferous, and Permian Research: Stratigraphy, Environments, Climate, and Resources. Filodiritto Editore–Proceedings*.
- MALINVERNO, A., ERBA, E. & HERBERT, T.D. 2010. Orbital tuning as an inverse problem: Chronology of the early Aptian oceanic anoxic event 1a (Selli Level) in the Cismon APTICORE. *Paleoceanography* 25, PA2203. DOI 10.1029/2009PA001769
- MENEGATTI, A.P., WEISSERT, H., BROWN, R.S., TYSON, R.V., FARRIMOND, P., STRASSER, A. & CARON, M. 1998. High-resolution $\delta^{13}\text{C}$ stratigraphy through the early Aptian “Livello selli” of the Alpine tethys. *Paleoceanography* 13, 530–545. DOI 10.1029/98PA01793
- MEYER, K.M. & KUMP, L.R. 2008. Oceanic Euxinia in Earth History: Causes and Consequences. *Annual Review of Earth and Planetary Sciences* 36, 251–288. DOI 10.1146/annurev.earth.36.031207.124256
- MOOSAVIZADEH, M.A., MAHBOUBI, A., MOUSSAVI-HARAMI, R.M.A. & KAVOOSI, M.A., 2014. Early Aptian Oceanic Anoxic Event (OAE 1a) in moderately Arabian Plate Setting: An Example from Dariyan Formation in Zagros Fold-Trust Belt, SE Iran. *Arabian Journal of Geosciences* 7, 4745–4756. DOI 10.1007/s12517-013-1025-z
- MÜLLER, G. 1969. Index of geo-accumulation in Sediments of the Rhine River. *Geojournal* 2, 108–118.

- MURRAY, J.W. 1989. Syndepositional dissolution of calcareous foraminifera in moder shallow-water sediments. *Marine Micropaleontology* 15, 117–121.
DOI /10.1016/0377-8398(89)90007-8
- MURRAY, J.W. 2006. *Ecology and Applications of Benthic Foraminifera*. 400 pp. Cambridge University Press, New York. DOI 10.1017/CBO9780511535529
- MURRAY, J.W. & ALVE, E. 1999. Natural dissolution of modern shallow water benthic foraminifera: Taphonomic effects on the palaeoecological record. *Palaeoecology, Palaeogeography, Palaeoclimatology* 146, 195–209.
- NOZAKI, T., KATO, YA. & SUZUKI, K. 2013. Late Jurassic ocean anoxic event: evidence from voluminous sulfide deposition and preservation in the Panthalassa. *Scientific Reports* 3(1889), 1–6.
- OLFERIEV, A.G., BENIAMOVSKI, V.N., VISHNEVSKAYA, V.S., IVANOV, A.V., KOPAEVICH, L.F., OVECHKINA, M.N., PERVUSHOV, E.M., SEL'TSER, V.B., TESAKOVA, E.M., KHARITONOV, V.M. & SHCHERBININA, E.A. 2008. Upper Cretaceous deposits in the northwest of Saratov Region, Part 2: Problems of chronostratigraphy and regional geological history. *Stratigraphy and Geological Correlation* 16, 267–294.
DOI 10.1134/S0869593808030040
- OLSZEWSKI, T.D. 2004. Modeling the influence of taphonomic destruction, reworking, and burial on time-averaging in fossil accumulations. *Palaios* 19, 39–50.
DOI 10.1669/0883-1351(2004)019<0039:MTIOTD>2.0.CO;2
- OSCHMANN, W. 2011. Black shales, 201–210. REITNER, J. & THIEL, V. (eds) *Encyclopedia of Geobiology*. Dordrecht, Springer Science+Business Media B.V.
DOI 10.1007/978-1-4020-9212-1_37
- PARK, M.-H., KIM, I.-S. & RYU, B.-J. 2003. Framboidal pyrites in late Quaternary core sediments of the East Sea and their paleoenvironmental implications. *Geosciences Journal* 7(3), 209–215. DOI 10.1007/BF02910287
- PERCIVAL, L.M.E., TEDESCHI, L.R., CREASER, R.A., BOTTINI, C., ERBA, E., GIRAUD, F., SVENSEN, H., SAVIAN, J., TRINDADE, R., COCCIONI, R., FRONTALINI, F., JOVANE, L., MATHER, T.A. & JENKYN, H.C. 2021. Determining the style and provenance of magmatic activity during the Early Aptian Oceanic Anoxic Event (OAE 1a). *Global and Planetary Change* 200, 103461. DOI 10.1016/j.gloplacha.2021.103461
- POŃAVIČ, M., PAŠAVA, L., VYMAZALOVÁ, A., KRÍBEK, B., DENG, H., LUO, T., LI, C. & ZENG, M. 2006. Fractionation of toxic trace elements in soils around Mo-Ni black shale-hosted mines, Zunyi region, southern China: Environmental implications. *Bulletin of Geosciences* 81, 197–206.
DOI 10.3140/bull.geosci.2006.03.197
- PREMOLI SILVA, I., ERBA, E., SALVINI, G., LOCATELLI, C. & VERGA, D. 1999. Biotic changes in Cretaceous oceanic anoxic events of the Tethys. *Journal of Foraminiferal Research* 29, 352–370.
- RIMMER, S.M., THOMPSON, J.A., GOODNIGHT, S.A. & ROBL, T.L. 2004. Multiple controls on the preservation of organic matter in Devonian–Mississippian marine black shales: geochemical and petrographic evidence. *Palaeogeography, Palaeoclimatology, Palaeoecology* 215, 125–154.
DOI 10.1016/S0031-0182(04)00466-3
- RUDNICK, R.L. & GAO, S. 2003. Composition of the Continental Crust. *Treatise on Geochemistry* 3, 1–64. Elsevier, Amsterdam. DOI 10.1016/B0-08-043751-6/03016-4
- SAWLOWICZ, Z. 1993. Pyrite framboids and their development: a new conceptual mechanism. *Geologische Rundschau* 82, 148–156. DOI 10.1007/BF00563277
- SCOTESE, C.R. 2014. *The PALEOMAP Project PaleoAtlas for ArcGIS, version 2, Vol. 2, Cretaceous Plate Tectonic, Paleogeographic, and Paleoclimatic Reconstructions*. Maps 16–32. PALEOMAP Project, Evanston, IL.
- SCOTESE, C.R. 2016. *Some Thoughts on Global Climate Change: The transition from Icehouse to Hothouse, in the Earth History: The evolution of the Earth System*. PALEOMAP Project, Evanston, IL.
- SCHLANGER, S.O. & JENKYN, H.C. 1976. Cretaceous oceanic anoxic events: causes and consequences. *Geologieen Mijnbouw* 55, 179–184.
- TAYLOR, G.R. 1983. A mechanism for framboid formation – The role of bacteria. *Mineralium Deposita* 18, 129–130.
DOI 10.1007/BF00206701
- TEJADA, M.L.G., SUZUKI, K., KURODA, J., COCCIONI, R., MAHONEY, J.J., OHKOUCHI, N., SAKAMOTO, T. & TATSUMI, Y. 2009. Ontong Java Plateau eruption as a trigger for the early Aptian oceanic anoxic event. *Geology* 37, 855–858.
DOI 10.1130/G25763A.1
- TRABUCHO-ALEXANDRE, J., HAY, W.W. & DE BOER, P.L. 2012. Phanerozoic environments of black shale deposition and the Wilson Cycle. *Solid Earth* 3, 29–42.
DOI 10.5194/se-3-29-2012
- TRIBOVILLARD, N., ALGEO, T.J., LYONS, T. & RIBOULLEAU, A. 2006. Trace-metals as paleoredox and paleoproductivity proxies: an update. *Chemical Geology* 232, 12–32.
DOI 10.1016/j.chemgeo.2006.02.012
- ULMISHEK, G. 2003. Petroleum geology and resources of the West Siberian basin, Russia. *U.S.G.S. Bulletin* 2201-G, 49.
- VAN BREUGEL, Y., SCHOUTEN, S., TSIKOS, H., ERBA, E., PRICE, G.D. & SINNINGHE DAMSTÉ, J.S. 2007. Synchronous negative carbon isotope shifts in marine and terrestrial biomarkers at the onset of the early Aptian oceanic anoxic event 1a: Evidence for the release of ¹³C-depleted carbon into the atmosphere. *Paleoceanography* 22(1), PA1210.
DOI 10.1029/2006PA001341
- VINE, J.D. & TOURTELLOT, E.B. 1970. Geochemistry of black shale deposit ± a summary report. *Economic Geology* 65, 253–272.
DOI 10.2113/gsecongeo.65.3.253
- VON BARGEN, D. & LEHMANN, J. 2014. Benthic ecosystem response to the deposition of lower Aptian black shales in an epicontinental sea. *Cretaceous Research* 51, 208–224.
DOI 10.1016/j.cretres.2014.06.006
- VODYANITSKII, YU.N. 2012. Standards for the contents of heavy metals and metalloids in soils. *Eurasian Soil Science* 45, 321–328. DOI 10.1134/S1064229312030131
- WANG, L., SHI, X. & JIANG, G. 2012. Pyrite morphology and redox fluctuations recorded in the Ediacaran Doushantuo Formation. *Palaeogeography, Palaeoclimatology, Palaeoecology* 333, 218–227. DOI 10.1016/j.palaeo.2012.03.033
- WESTERMANN, S., STEIN, M., MATERA, V., FIET, N., FLEITMANN, D.,

- ADATTE, T. & FÖLLMI, K.B. 2013. Rapid changes in the redox conditions of the western Tethys Ocean during the early Aptian oceanic anoxic event. *Geochimica et Cosmochimica Acta* 121, 467–486. DOI 10.1016/j.gca.2013.07.023
- WIGNALL, P.B. & MYERS, K.J. 1988. Interpreting the benthic oxygen levels in mudrocks: a new approach. *Geology* 16, 452–455. DOI 10.1130/0091-7613(1988)016<0452:IBOLIM>2.3.CO;2
- WIGNALL, P.B. & TWITCHETT, R.J. 1996. Oceanic anoxia and the end Permian mass extinction. *Science* 272, 1155–1158. DOI 10.1126/science.272.5265.1155
- WIGNALL, P.B., NEWTON, R. & BROOKFIELD, M.E. 2005. Pyrite framboid evidence for oxygen-poor deposition during the Permian-Triassic crisis in Kashmir. *Palaeogeography, Palaeoclimatology, Palaeoecology* 216, 183–188. DOI 10.1016/j.palaeo.2004.10.009
- WIGNALL, P.B., BOND, D.P.G., KUWAHARA, K., KAKUWA, Y., NEWTON, R.J. & POULTON, S.W. 2010. An 80 million year oceanic redox history from Permian to Jurassic pelagic sediments of the Mino-Tamba terrane, SW Japan, and the origin of four mass extinctions. *Global and Planetary Change* 71, 109–123. DOI 10.1016/j.gloplacha.2010.01.022
- WILKIN, R.T. & BARNES, H.L. 1997. Formation processes of framboidal pyrite. *Geochimica et Cosmochimica Acta* 61(2), 323–339. DOI 10.1016/S0016-7037(96)00320-1
- WILKIN, R.T., BARNES, H.L. & BRANTLEY, S.L. 1996. The size distribution of framboidal pyrite in modern sediments: An indicator of redox conditions. *Geochimica et Cosmochimica Acta* 60, 3897–3912. DOI 10.1016/0016-7037(96)00209-8
- YANKO, V., ARNOLD, A.J. & PARKER, W.C. 1999. Effects of Marine Pollution on Benthic Foraminifera, 217–235. SEN GUPTA, B.K. (ed.) *Modern Foraminifera*. Kluwer Academic Publisher, Dordrecht. DOI 10.1007/0-306-48104-9_13
- ZAKHAROV, YU.D., BARABOSHKIN, E.YU., WEISSERT, H., MICHAILOVA, I.A., SMYSHLYAEVA, O.P. & SAFRONOV, P.P. 2013. Late Barremian-early Aptian climate of the northern middle latitudes: Stable isotope evidence from bivalve and cephalopod mollusks of the Russian Platform. *Cretaceous Research* 44, 183–201. DOI 10.1016/j.cretres.2013.04.007
- ZORINA, S.O. 2007. Stratigraphy of middle-upper Jurassic deposits in the East Russian plate. *Stratigraphy and Geological Correlation* 15, 267–276. DOI 10.1134/S0869593807030033
- ZORINA, S.O. 2009. Sequence stratigraphy of Lower Cretaceous deposit on the eastern Russian Plate. *Russian Geology and Geophysics* 50, 430–437. DOI 10.1016/j.rgg.2008.08.007
- ZORINA, S.O. 2014. Eustatic, tectonic, and climatic signatures in the Lower Cretaceous siliciclastic succession on the Eastern Russian Platform. *Palaeogeography, Palaeoclimatology, Palaeoecology* 412, 91–98. DOI 10.1016/j.palaeo.2014.07.029
- ZORINA, S.O. 2016. Sea-level and climatic controls on Aptian depositional environments of the Eastern Russian Platform. *Palaeogeography, Palaeoclimatology, Palaeoecology* 441, 599–609. DOI 10.1016/j.palaeo.2015.08.035
- ZORINA, S. 2019. Early Cretaceous microfascies and paleobathymetry in the Eastern Russian Platform, 288–292. In NOURGALIEV, D.K. (ed.) *Sedimentary Earth Systems: Stratigraphy, Geochronology, Petroleum Resources. Proceedings Kazan Golovkinsky Stratigraphic Meeting, 2019*. Filodiritto Editore – Proceedings.
- ZORINA, S.O. & STARTSEVA, G.N. 2010. Biofacies of benthic foraminifers and paleobathymetry and sequence stratigraphy of Middle Jurassic–Lower Cretaceous deposits on the eastern Russian Plate (area of the Tatarsko–Shatrashanskaya 1 borehole, Republic of Tatarstan). *Litosfera* 4, 81–93.
- ZORINA, S.O., PAVLOVA, O.V., GALIULLIN, B.M., MOROZOV, V.P. & ESKIN, A.A. 2017. Euxinia as a dominant process during OAE1a (Early Aptian) on the Eastern Russian Platform and during OAE1b (Early Albian) in the Middle Caspian. *Science China: Earth Sciences* 60, 58–70. DOI 10.1007/s11430-016-0043-1
- ZORINA, S.O., NIKASHIN, K.I. & SOKERIN, M.Y. 2020. Geochemical Indicators of “Camouflaged” Pyroclastic Material in the Upper Jurassic-Lower Cretaceous Deposits of the Eastern Russian Platform. *Doklady Earth Sciences* 493, 608–611. DOI 10.1134/S1028334X2008022X